ADVANCED FUNCTIONAL MATERIALS
www.afm-journal.de

Beetle-Inspired Gradient Slant Structures for Capacitive Pressure Sensor with a Broad Linear Response Range

Lei Wu, Xuan Li, Jungrak Choi, Zhi-Jun Zhao, Linmao Qian, Bingjun Yu, and Inkyu Park**

Flexible pressure sensors with broad linearity range and excellent sensor-to-sensor uniformity have attracted unprecedented attention in the electronic skins, human–machine interfaces, and environmental monitoring. However, challenges including poor sensor-to-sensor uniformity owing to the randomness of the used nanomaterials or porous structures and saturated response that leads to a restricted linearity range because of structural stiffening have been yet addressed. Herein, a novel dielectric layer based on beetle-inspired gradient slant structures (GSS) is proposed to endow capacitive pressure sensors with extensive linearity range and excellent sensor-to-sensor uniformity. The excellent compressibility of the GSS due to the bending deformation of the slant pillars significantly enhances sensor sensitivity. The broad linearity range comes from the compensation of contact area during sequential contact of the GSS dielectric layer from tall to low slant pillars with electrodes. The high sensor-to-sensor uniformity is ascribed to the excellent batch-to-batch consistency of prepared GSS via 3D printing-based fabrication process. Moreover, the proposed GSS-based pressure sensors present rapid response/recovery, low detection limit, excellent dynamic response, negligible hysteresis, and outstanding long-term stability. Finally, the excellent applicabilities of proposed capacitive pressure sensors in diverse scenarios including external pressure stimuli detection, a flexible perception array, and a smart insole system are demonstrated.

1. Introduction

With the flourishing progress of the Internet of Things and artificial intelligence, flexible pressure sensors have triggered unprecedented attention owing to their promising applications in the electronic skins, human-machine interfaces, and environmental monitoring.[1–5] According to the working mechanism, the flexible pressure sensors are cataloged into four common types including piezo-electric, piezoresistive, piezo-capacitive, and triboelectric type.[6–8] Among them, capacitive-type sensors that converted pressure stimuli into capacitance signals have attracted increasing attention because of their simple structure, low power consumption, temperature insensitivity, and fast response.[9–11] In general, there are different magnitudes of external pressure stimuli in diverse application scenarios. For example, a subtle pressure (<1 kPa) and medium pressure (>1 kPa) are generated during the respiration and gentle touches, respectively[12]; plantar foot pressure often produces higher pressure (>10 kPa).[13] Meanwhile, a linear response is necessary to simplify data processing and implement delicate monitoring.[14] In addition, high sensor-to-sensor reproducibility and low hysteresis are of significance to any practical applications.[15] To this end, flexible capacitive pressure sensors are demanded with a wide linear response range and high sensor-to-sensor reproducibility to adapt diverse application scenarios.[16–18]

Microstructured dielectric or electrode layer is an effective strategy to improve the sensing performance of capacitive-type pressure sensors.[19] This is because that these microstructures not only can reduce the effective Young's modulus and thereby enhance the compressibility, but also decrease the viscoelasticity by introducing the air.[20] Bao et al.[21] first introduced micropyramid arrays in dielectric layer and achieved a high sensitivity of 0.55 kPa^{-1}, which is 30 times higher than that of capacitive sensor with unstructured dielectric layer, within a pressure range of 2 kPa. Since then, a wide variety of surface and internal microstructures including needles, pillars, cones, wrinkles, and porous structures were designed and developed as dielectric layers.[22–26] However, these pressure sensors based on microstructured dielectric layer present a restricted linear sensing range because structural stiffening gives rise to signal saturation. Recently, gradient microstructures have become a promising dielectric layer to further improve the sensitivity and linear sensing range.[27,28] For instance, Bai et al.[29] introduced graded

L. Wu, L. Qian, B. Yu
Tribology Research Institute
State Key Laboratory of Traction Power
Southwest Jiaotong University
Chengdu 610031, China
E-mail: bingjun@swjtu.edu.cn
X. Li, J. Choi, I. Park
Department of Mechanical Engineering
Korea Advanced Institute of Science and Technology (KAIST)
Daejeon 34141, Republic of Korea
E-mail: inkyu@kaist.ac.kr
Z.-J. Zhao
Institute of Smart City and Intelligent Transportation
Southwest Jiaotong University
Chengdu 611756, China

The ORCID identification number(s) for the author(s) of this article can be found under https://doi.org/10.1002/adfm.202312370

DOI: 10.1002/adfm.202312370

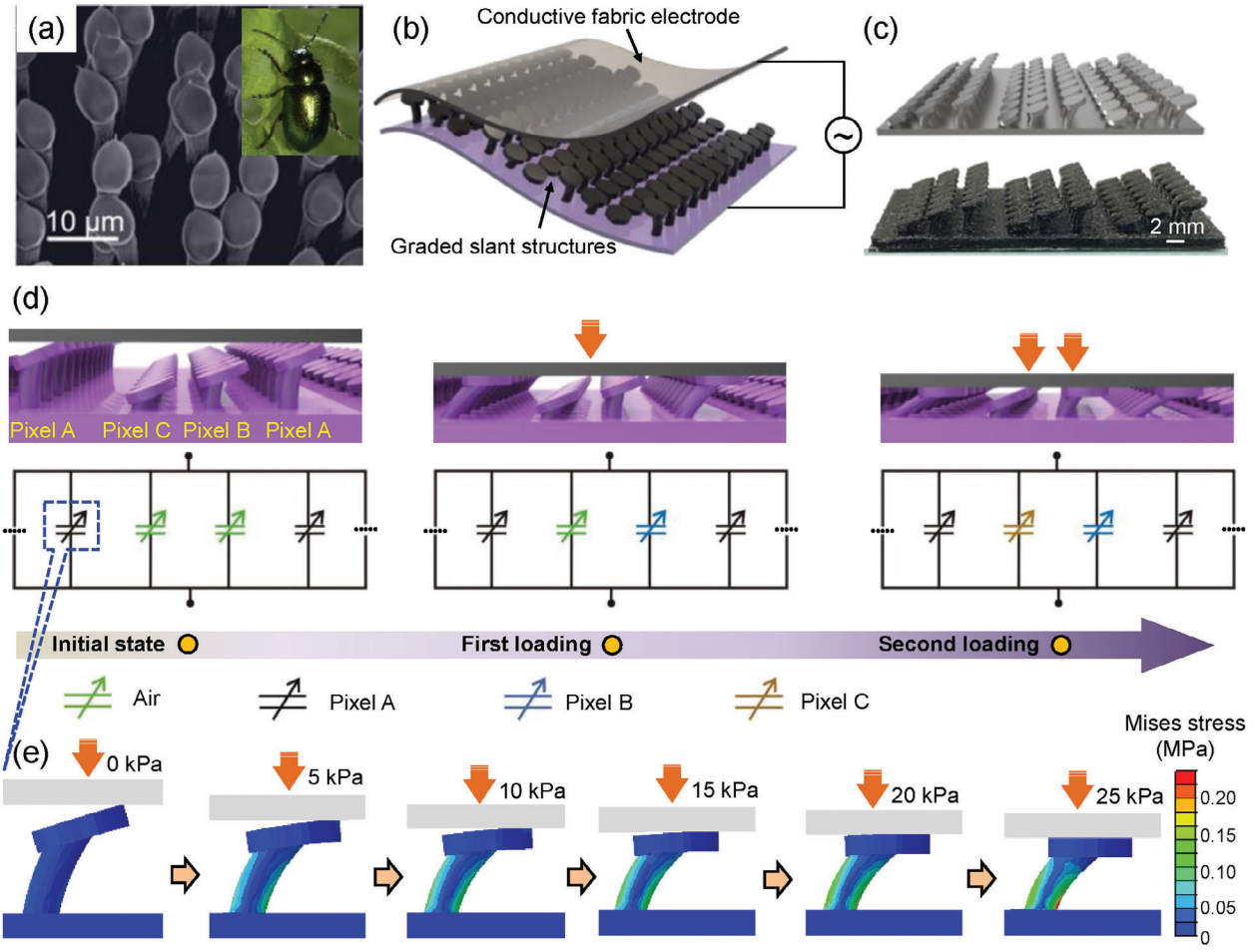

Figure 1. The structure design and working mechanism of the proposed capacitive pressure sensor. a) The surface topography of adhesive hair of a dock beetle.[31] b) Schematic of capacitive pressure sensor based on the beetle-inspired GSS dielectric layer. c) Schematic illustration and optical image of the GSS dielectric layer. d) Schematic illustration of working mechanism. e) FEA simulation results regarding the deformation behavior of single slant pillar under the increasing pressure.

intrafillable microstructures duplicated by the sandpaper in the dielectric layer, and such a strategy can significalty enhance the sensitivity and sensing range. However, they could feature low sensor-to-sensor uniformity owing to the poor batch-to-batch consistency of random structures. Li et al.[30] reported a wide-range pressure sensor based on a graded inclined-tip cone array, but it delivers an unsatisfactory linearity. Therefore, realizing capacitive pressure sensors with broad linearity range and high sensor-to-sensor uniformity remains a huge challenge.

In this paper, mimicking the structure of a beetle foot (**Figure 1a**),[31] a novel dielectric layer based on beetle-inspired gradient slant structures (GSS) is proposed to endow the capacitive pressure sensors with extensive linearity range. Given that the GSS dielectric layer undergoes the bending deformation instead of compression deformation, the constructed pressure sensors exhibit an excellent compressibility, significantly enhancing the sensor sensitivity. Moreover, the slant pillars with different heights can sequentially contact the electrode with the increasing pressure, which can effectively address the signal saturation because of structural stiffening, thereby increasing the linear sensing range. The excellent batch-to-batch consistency of fabricated GSS dielectric layer endows the high sensor-to-senor uniformity. Finite element analysis (FEA) simulation for the deformation behavior of the GSS was performed to further confirm the working mechanism. Furthermore, the proposed GSS-based capacitive pressure sensors were demonstrated to exhibit a rapid response/recovery, a low detection limit, an excellent dynamic response, a negligible hysteresis, and an outstanding long-term stability. Finally, the pressure sensors were successfully applied in diverse scenarios including external pressure stimuli detection, a flexible perception array, and a smart insole system.

2. Results and Discussion

2.1. Structure Design and Working Principle of Proposed Capacitive Pressure Sensor

Figure 1b schematically displays the proposed capacitive pressure sensor with sandwich features, which consisits of a GSS dielectric layer and two parallel conductive fabric electrodes (Figure S1 of Supporting Information). The dielectric layer was designed as three types of slant pillar pixels with an identical tilted angle

and different heights (Figure 1c), where the slant pillars with the tallest, medium, and lowest heights were denoted as pixels A, B, and C, respectively. The GSS dielectric layer was prepared by 3D printing and subsequent dissolution in the DI water, as demonstrated in Figure S2 (Supporting Information) (The details can be seen from the Experimental Section). The carbon nanotubes (CNTs) were applied as conductive filters to enhance the dielectric constant of solid elastomer because they can significantly reduce the percolation threshold.[32]

Figure 1d depicts the working mechanism of the GSS-based capacitive pressure sensor. At low pressure, the relatively low slant pillars (pixels B and C) are separated from the top electrodes, thus they are connected to the air in series, thereby rendering limited contributions for the capacitance value of the pressure sensor. In this state, the dielectric behavior of the GSS is dominated by the pixels A. It is well known that the capacitance can be expressed as $C = \epsilon A/d$, where the ϵ denotes the permitivity, d is the distance between the two parallel electrodes, and A refers to the contact area of the dielectric layer with the electrode.[27] For high-k dielectric layer, the variations in the capacitance of pressure sensor are dominated by the contact area.[28] With the increasing pressure, the two parallel electrodes gradually approach, resulting in the deformation of the tallest slant pillars. The FEA method was applied to simulate the deformation behavior of single slant pillar. Figure 1e presents the simulation results under different external pressure of 5, 10, 15, 20, and 25 kPa. As the applied pressure increases to be 25 kPa, the slant pillar undergoes bending deformation, and the contact area with top electrode gradually increases, which could dominate in the increasing capacitance vaules of the pressure sensor. With further increasing pressure, the relatively low slant pillars (pixels B and C) sequentially contact the top electrodes, thus they are parallelly connected with pixels A (Figure 1d). In this state, the capacitance variations are determined by the pixels B and C, and the contact area of the GSS dielectric layer with top electrode can be superimposed in sequence with the increasing pressure (Figure 1f). The variations in the contact area play a role in the continuous rise of capacitance values within the pressure sensor based on the GSS. This contributes significantly to resolving problems of signal saturation that arise from micro/nanostructures with uniform height. As a result, this technology achieves a capacitive response across an extensive sensing range.

2.2. FEA Simulation and Experimental Characterization of Capacitive Pressure Sensor

The deformation behavior of the GSS dielectric layer was simulated using the FEA method. At relatively low pressure (0–30 kPa), only the tallest slant pillars (pixels A) contact the top electrode, and the contact area is positively correlated with applied pressure (**Figure** 2a). With further increasing pressure, the pixels B come into contact with the electrode, and the contact area gradually increases. When the pressure reaches 70 kPa, the pixels C contact the top electrode. Such results further demonstrate that the gradient slant pillars can sequentially contact the top electrode, which can effectively address the signal saturation of capacitive pressure sensor based on uniform structures with consistent height. Therefore, the superimposed contact area under different pressure regions can realize linear response over an extensive sensing range. It is also noted that the GSS mainly undergo bending deformation instead of compressive deformation. This characteristic greatly amplifies the sensitivity of pressure sensors due to their remarkable compressibility.

The capacitive response of the pressure sensors was characterized using an experimental setup consisting of a high-precision universal testing machine, an LCR meter, and a personal computer (Figure 2b). The capacitive sensor sensitivity (S) can be expressed as $S = \delta(\Delta C/C_0)/\Delta P$, where the C_0 and $\Delta C = (C - C_0)$ refer to the initial capacitance and the capacitance change under external pressure stimuli, respectively. Figure 2c compares the normalized capacitive response of the pressure sensors based on gradient slant pillars and three types of uniform slant pillars (the corresponding topographies can be seen in Figure S3, Supporting Information). These results indicate that the GSS-based capacitive pressure sensor exhibits an extensive linearity range (130 kPa) with a sensitivity of 0.12 kPa^{-1}, which significantly surpasses those of capacitive pressure sensors based on uniform slant pillars with consistent height, demonstrating the superiority of the proposed GSS-based pressure sensors.

To demonstrate that the contact area of GSS dielectric layer affected the sensor performance, the normalized capacitive response of the pressure sensors based on the graded slant pillars with a tilted surface or a flat surface at the top was further investigated. Compared with pressure sensor based on graded slant pillars with a tilted surface at the top, that with a flat surface at the top presented an unsatisfactory linearity (Figure S4, Supporting Information). Sudden changes in capacitance signals were observed at two pressure levels, and this could be attributed to a sharp increase in contact area when the upper electrode contacted with pixel B and pixel C in sequence. It indicated that the capacitive response of pressure sensor was tightly related with the geometry of contact area of dielectric layer, and controlling the contact area can achieve a desired linear response, which is consistent with the reported literatures.[28,33]

Owing to its high viscosity, the PDMS prepolymer solution with a high CNT concentration is difficult to flow into the printed molds.[34] Therefore, the CNT concentration selected in this paper is not above 1.0 wt% to ensure fabrication quality of the GSS. Figure 2d displays the normalized capacitive response of GSS-based pressure sensor with various weight percentages of CNTs (0–1.0 wt%). At each CNT concentration, the GSS-based sensors exhibit an excellent linearity within the pressure range of 130 kPa. Moreover, the pressure sensor with a 1.0 wt% CNTs presents a maximum sensitivity (0.12 kPa^{-1}), which is three times higher than that those without CNT fillters (Figure S5, Supporting Information). These results indicated that increasing or decreasing CNT concentration only changed the sensor sensitivity, while did not alter the sensing range. Therefore, the CNT concentration of 1.0 wt% was selected as the GSS dielectric layer for the following experiments.

The compressive modulus of dielectric layer dominates in the sensor performance including sensing range and sensitivity, and it is determined by and microstructure geometry and layout.[35] The effect of structural parameters of slant pillars, such as tilted angle and the thickness, on the sensor response was studied. Figure 2e displays the normalized capacitive response of the pressure sensors based on the GSS with identical thickness

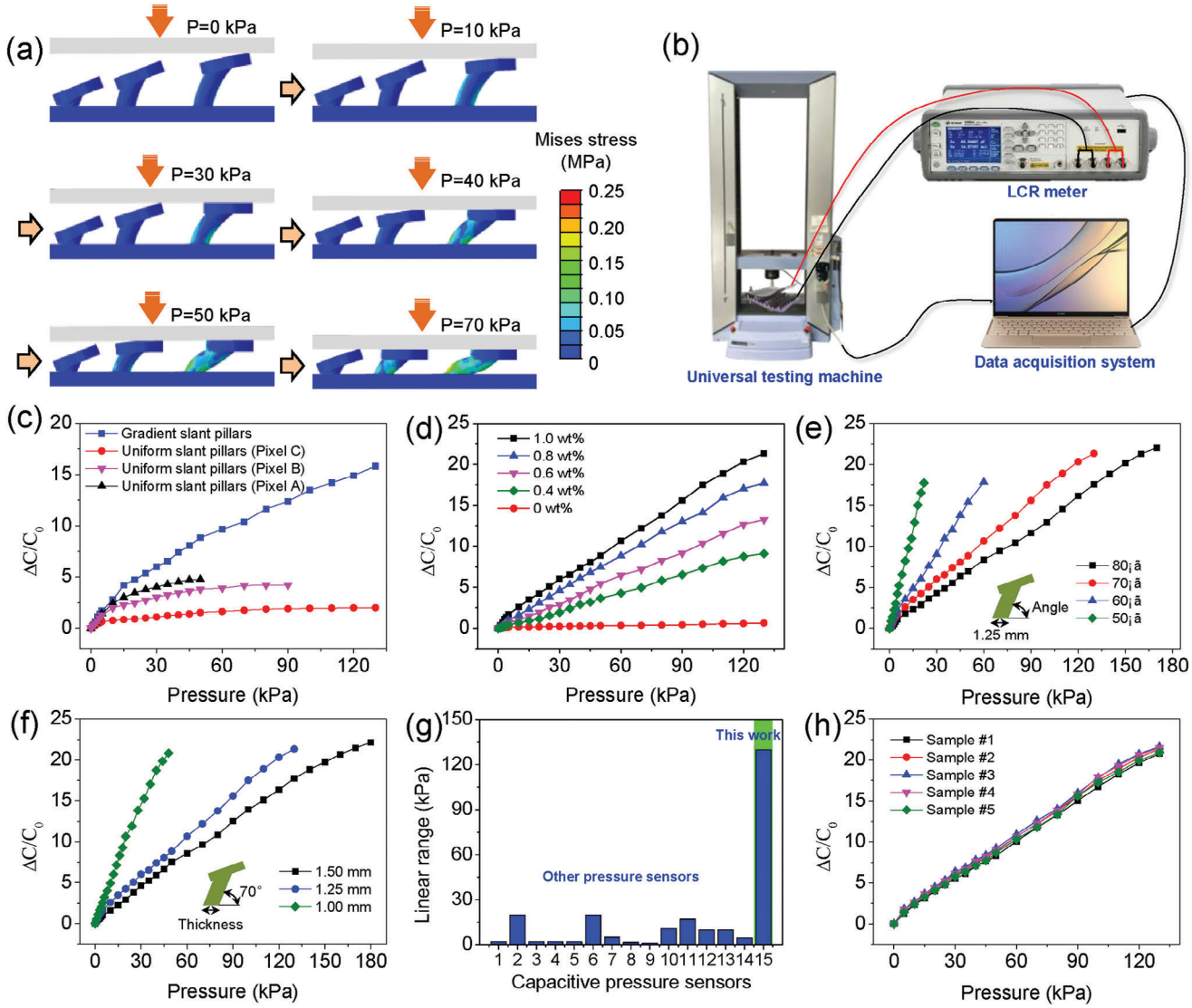

Figure 2. FEA simulation and experimental characterization of the capacitive pressure sensors. a) FEA simulation results regarding the deformation behavior of the GSS dielectric layer under the increasing pressure. b) Experimental setup for characterizing the capacitive response. c) The normalized capacitive response of the pressure sensors based on the gradient slant pillars or three types of uniform slant pillars with consistent height. The tilted angle and the thickness of slant pillars are fixed as 70° and 1.25 mm, respectively. Here, the CNT content of 0.8 wt% was applied. d) The normalized capacitive response of the GSS-based pressure sensors with different weight percentages of CNTs (0, 0.4, 0.6, 0.8, and 1.0 wt%). e, f) The relative capacitance changes versus the pressure for GSS-based pressure sensors with different tilting angles and thickness. g) Comparison of linear sensing range of the GSS-based pressure sensors with the reported capacitive pressure sensors. h) Relative capacitance changes of five fabricated GSS-based pressure sensors.

(1.25 mm) and different tilted angles of 50°, 60°, 70°, and 80° (the surface topographies are shown in Figure S6, Supporting Information). As the tilted angle increases from 50° to 80°, the linear sensing range gradually increases from 22 to 170 kPa, while the sensitivity degrades from 0.81 to 0.13 kPa^{-1}. Figure 2f displays the normalized capacitive response of the pressure sensors based on the GSS with identical tilted angle (70°) and different thickness of 1.00, 1.25, and 1.50 mm (the surface topographies are shown in Figure S7, Supporting Information). With the increasing thickness from 1.0 to 1.5 mm, the sensing range increases from 48 to 180 kPa, while the sensitivity gradually degrades from 0.43 to 0.12 kPa^{-1}. Further analysis deduced that when increasing tilted angle or thickness, the bending deformation of slant pillars were more difficult, thus the dielectric layer exhibited larger compressive modulus, thereby increasing the sensing range. Furthermore, effects of inter-pillar spacing including *X* and *Y* directions (The definition can be seen in Figure S8, Supporting Information) on the sensitivity and linearity of the pressure sensor were further investigated. As the inter-pillar spacing in the X direction increased, the sensitivity significantly increased, while linear sensing range degraded, as shown in Figure S9a (Supporting Information). With the increase of inter-pillar spacing in the *Y* direction from 3.5 to 5.5 mm, the linear sensing range decreased from 130 to 40 kPa, and the sensitivity increased from

0.164 to 0.296 kPa^{-1} (Figure S9b, Supporting Information). It indicated that the sensor linearity did not relate with the interpillar spacing, while sensor sensitivity gradually increased with the increase of the interpillar spacing, which can be ascribed as the increasing compressibility. The above results indicate that the proposed pressure sensors exhibit an extensive linear sensing range with moderate sensitivity compared with previously reported capacitive pressure sensors (Figure 2g and Table S1, Supporting Information).[21–24,32,36–45]

Considering that the service environment of the sensor is complex, it is necessary to investigate the effects of environmental temperature and humidity on sensor response. Figure S10 (Supporting Information) displays the normalized capacitive response of the GSS-based pressure sensor under 60 kPa at different temperature and relative humidity. As the environmental temperature changes from 20 °C to 60 °C, the capacitance variation is less than 5% (Figure S10a, Supporting Information). When the relative humidity ranges from 30% to 90%, the relative capacitance changes remain stable (Figure S10b, Supporting Information). Therefore, the proposed GSS-based capacitive sensors have advantages of temperature and humidity inertness, thereby ensuring effective and accurate sensing in complex environments. In addition, the normalized capacitive response for five fabricated GSS-based sensors was investigated to confirm the high sensor-to-sensor uniformity. The sensitivity and linear sensing range of the pressure sensors exhibit a remarkable reproducibility with the RSD of 3.0% (Figure 2h), which can be ascribed as the excellent batch-to-batch consistency of the prepared GSS dielectric layer through 3D printing-based process.

2.3. Sensing Performances of GSS-Based Capacitive Pressure Sensor

The sensing performances of the proposed GSS-based sensor with a sensitivity of 0.12 kPa^{-1} and a linear range of 130 kPa were studied. **Figure 3**a,b demonstrates the detection of capacitance response when the sensor is subjected to the pre-loading pressure of 1, 10, and 100 kPa. In general, when a small preload pressure of 1 kPa was applied to the GSS-based sensor, a tiny capacitance change (0.1 kPa) can be clearly distinguished (Figure 3b). Meanwhile, even though the proposed GSS-based sensor was subjected to a large pre-load pressure of 100 kPa, it can still accurately detect relatively small capacitance changes (1 kPa), as evident in Figure 3a. These results indicated that the proposed GSS-based pressure sensor can preserve high resolution over entire pressure range, thereby ensuring effective detection over a wide range. To investigate the dynamic response characteristic of the pressure sensors, the relative capacitance changes under the pressure of 1, 25, 60, and 120 kPa were characterized by five loading/unloading cycles. The results reveal a stable and reversible response at each applied pressure, as evident in Figure 3c. Moreover, the GSS-based sensor exhibits a short response-relaxation time (<46 ms) to external pressure stimuli (1 kPa), as evident in Figure 3d, further confirming an excellent dynamic response performance. The detection limit is the key parameter for detecting tiny pressure stimuli, such as air flow. A tiny pressure stimuli (<3 Pa) can be clearly identified by the pressure sensor (Figure 3e), indicating a low detection limit. The capacitive response of the GSS-based sensor during the loading/unloading process reveals a low hysteresis (<8%)[46] (Figure 3f). Furthermore, the pressure sensor was demonstrated to exhibit a stable capacitive response under 30 kPa at different vibration frequencies of 0.05, 0.2, 0.4, 1, and 4 Hz, as shown in Figure 3g. In addition, the sensor stability was investigated by 3000 loading/unloading cycles under 120 kPa. No obvious drift and degradation can be observed (Figure 3h), demonstrating an excellent long-term stability of the GSS-based pressure sensor.

2.4. Demonstrations of Practical Applications of GSS-Based Capacitive Pressure Sensor

Considering its excellent sensing performance, the proposed GSS-based pressure sensor was further applied in various scenarios including external pressure stimuli detection, a flexible perception array, and a smart insole system. Benefiting by its low detection limit, the GSS-based pressure sensor can detect the subtle air flow produced by a rubber suction bulb (**Figure 4**a). Similarily, the sensor can measure the mouth breathing-induced air movements, thereby applying for the real-time detection of human respiration state (Figure 4b and Video S1, Supporting Information). Figure 4c displays capacitive response of the pressure sensor fixed on the mouse under the condition of successive clicks. The single click and double click can be precisely recognized, demonstrating an exellent ability of the pressure sensor for detecting the external stimuli featured with extremely short time intervals. Furthermore, the applications of the GSS-based sensors in the field of wearable electronics were conducted. The pressure sensors were respectively fixed on the finger, wrist, and elbow, and a stretchable tape was covered on the surface of the GSS-based pressure sensor. Bending of the finger, wrist, and elbow caused the slant pillars to experience deformation due to the compression of the tape vertically. This compression resulted in altering the capacitance values of the pressure sensor. Video S2 (Supporting Information) demonstrates the application in real-time monitoring of the finger bending. Figure 4d further shows the capacitive response of the pressure sensor with respect to different bending angles. It indicates that the increase in the capacitance value can reflect the degree of finger bending. Similarily, the GSS-based sensors can detect the bending of the wrist and elbow, as shown in Figure 4e,f. To certify its application in electronic skins, the GSS-based pressure sensor was worn on the finger to compress the soft objects. As evident in Figure 4g–i, the pressure sensor can accurately and stably identify the gentle, medium, and high pressure touch.

Furthermore, a flexible perception array based on the GSS-based capacitive sensors was established to detect the spatial distribution of external pressure stimuli. **Figure 5**a and Figure S11 (Supporting Information) show the schematic of the designed measurement system of capacitive sensor array, which consisted of two analog multiplexers, a capacitance-to-digital converter, and an Arduino. The two 8-channel analog multiplexers were connected row channels and column channels in the sensor array, and they periodically selected channels. Accordingly, each capacitive pressure sensor in the flexible perception array can be cyclically scanned. The capacitance-to-digital converter was utilized

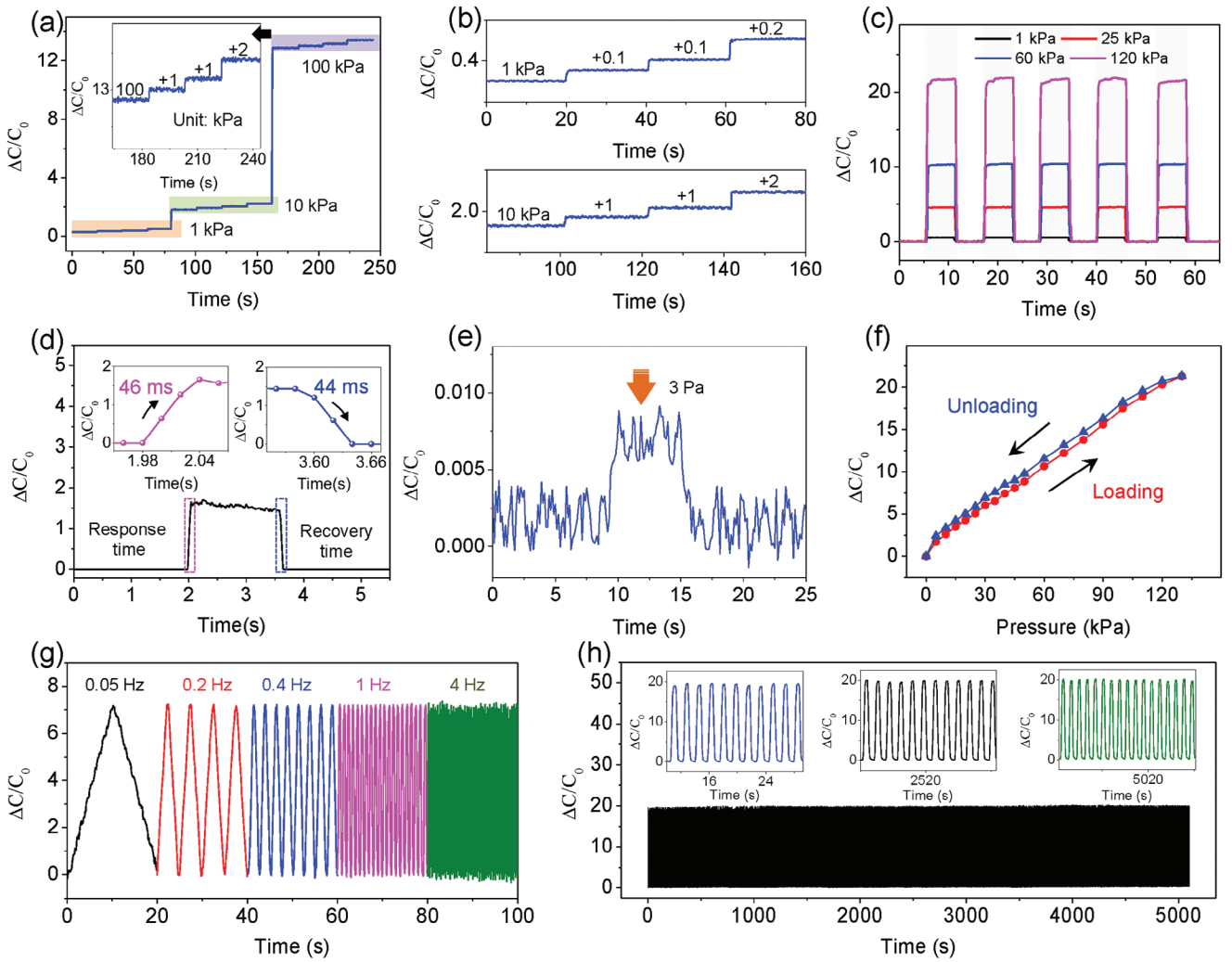

Figure 3. Sensing performance of the GSS-based capacitive pressure sensor. a,b) Detection of tiny pressure change when the sensor is subjected to preloading pressure of 1, 10, and 100 kPa. c) The normalized capacitive response under 1, 25, 60, and 120 kPa. d) The response-relaxation time of the pressure sensor. e) The relative capacitance change under a tiny pressure (3 Pa). f) The capacitive response of the GSS-based sensor during the loading/unloading process under 130 kPa. g) The sensor response at different vibration frequencies of 0.05, 0.2, 0.4, 1, and 4 Hz. h) Long-term stability tests of the sensor over 3000 loading/unloading cycles under 120 kPa.

to measure the capacitance values of pressure sensors, and an Arduino board was applied to data processing for monitoring capacitive signals in real time on a PC. Figure 5b displays a diagram of constructed flexible perception array with 5 × 5 matrix elements, which was composed of the GSS dielectric layer and two CNT–Ecoflex nanocomposite films as flexible electrode pads (Figure S12, Supporting Information). Even though the CNT network was embedded in the Ecoflex layer, the excellent current–voltage characteristics were detected (Figure S13, Supporting Information). When two objects with the weights of 0.5 and 6.0 g were placed on the perception array (Figure 5c), the size, position, and weight of the two objects could be accurately identified by the relative capacitance changes (Figure 5d). Furthermore, four 3D-printed letter blocks (“Z”, “H”, “K”, and “E”) were placed on the perception array (Figures 5e and S14, Supporting Information), and the corresponding pressure distribution maps were presented in Figure 5f. The results further indicate that the perception array can precisely detect the contours of letter blocks with negligible influence between adjacent cells.

The monitoring of plantar pressure distribution plays a key role in early disease diagnosis and correcting unhealthy postures.[13,47] A smart insole system consisting of seven capacitive pressure sensors on the sole, two CNT–Ecoflex nanocomposite films as flexible electrode pads (Figure S15, Supporting Information), two 4-channel capacitance-to-digital converters, and an Arduino was constructed. To comprehensively detect the plantar pressure distribution, the seven pressure sensors were mounted sequentially from the heel to toe, as shown in **Figure 6a**. Using the smart insole system, the static plantar pressure distribution under three different standing gaits (neutral, supination, and pronation) was investigated to provide guidelines for redressing unhealthy posture. As shown in Figure 6b, the normalized capacitive response of the seven pressure sensors in case of neutral gait are basically consistent, demonstrating a uniform

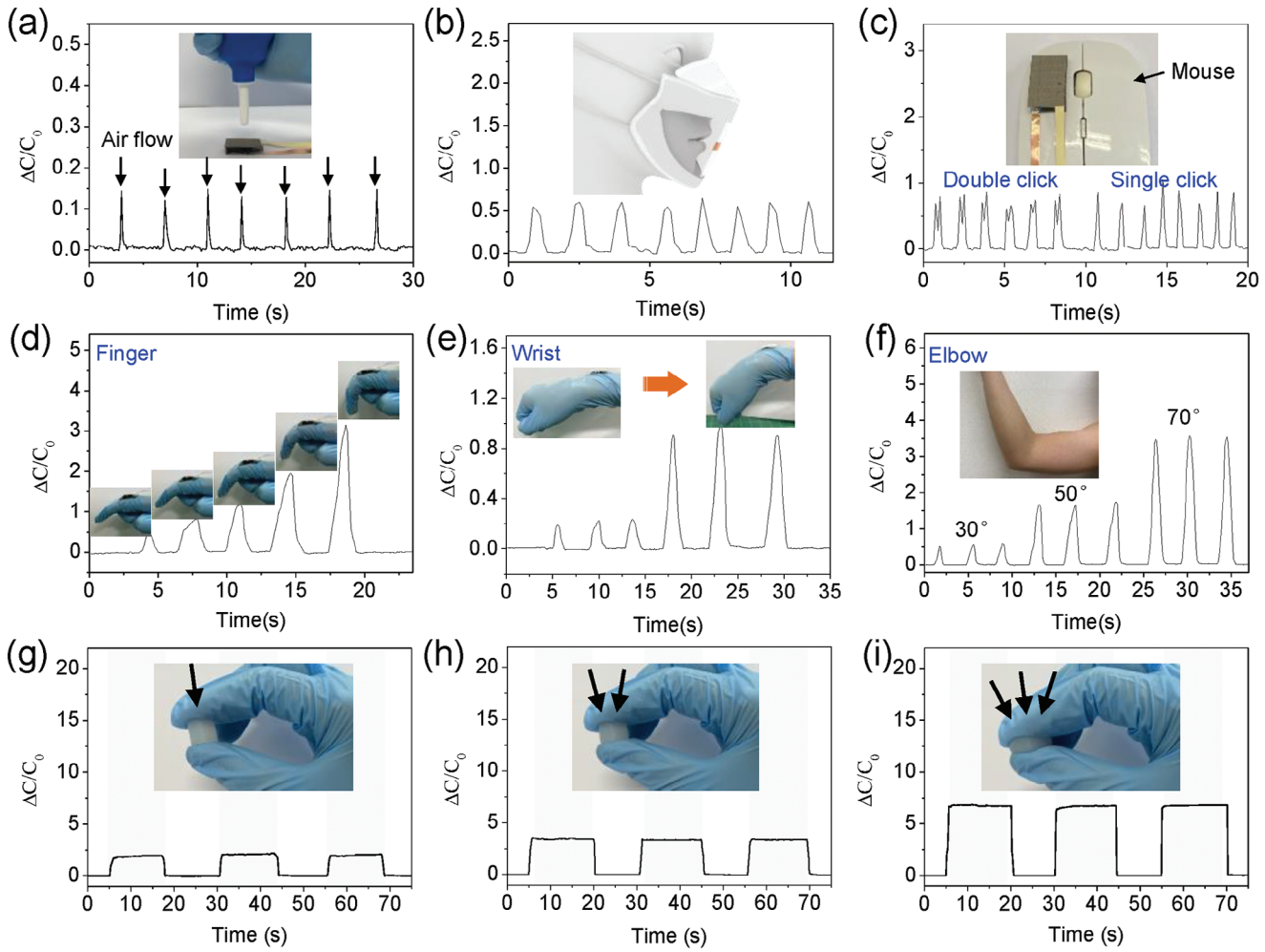

Figure 4. Demonstrations of the capacitive pressure sensor for detecting different external stimuli. a–c) Capacitance variations corresponding to air flow, respiration, and mouse click. d–f) Relative capacitance changes with respect to finger, wrist, and elbow flexion. g–i) Detection of the different compression for soft object.

distribution of plantar pressure. In comparison, for the two other standing gaits, distinct pressure distributions were clearly observed. In case of pronation gait, the relative capacitance changes of S3–S5 were lower than those of S1–S2 and S6–S8 (Figure 6c), which can be attributed that the pressure distributions of inside part were higher than those of outside part. For supination gait, the relative capacitance changes of S1–S4 were higher than those of S5–S7 (Figure 6d), which was ascribed to the higher-pressure distributions of the outside part compared to the inside part. These results demonstrate that static standing gaits can be distinguished by the constructed smart insole system.

In addition, the dynamic response of the smart insole system in continuous motion was investigated to demonstrate its applicability in sports activity monitoring. Video S3 (Supporting Information) demonstrates the application in real-time monitoring of the plantar pressure using the proposed GSS-based pressure sensor. Figure 6e illustrates a walking straight gait consisting of heel strike, mid stance, heel off, and toe off, and the corresponding plantar pressure distribution is displayed in Figure 6f. Figure 6g further displays the capacitive response of the seven pressure sensors during a gait cycle. The results reveal that the gravity center of the foot gradually changes from the heel to toe during a gait cycle. Furthermore, the established smart insole system was applied to monitor the evolution of plantar pressure distribution during the standing long jump consisting of pre-swing, jumping, take-off, heel strike, and standing. The histograms of relative capacitance changes indicate that the gravity center of the foot gradually changes from the toe to heel, and maximum pressure was obtained in the stage of heel strike (Figure 6h). Therefore, the smart insole system can be applied to precisely monitor the human motions.

3. Conclusions

In this paper, a novel dielectric layer based on the GSS was proposed to endow the capacitive pressure sensors with extensive linearity range and excellent sensor-to-sensor uniformity. The broad linearity range can be preserved from the compensation of contact area owing to sequential contact of the GSS from tall to low slant pillars with electrodes. Due to the excellent batch-to-batch

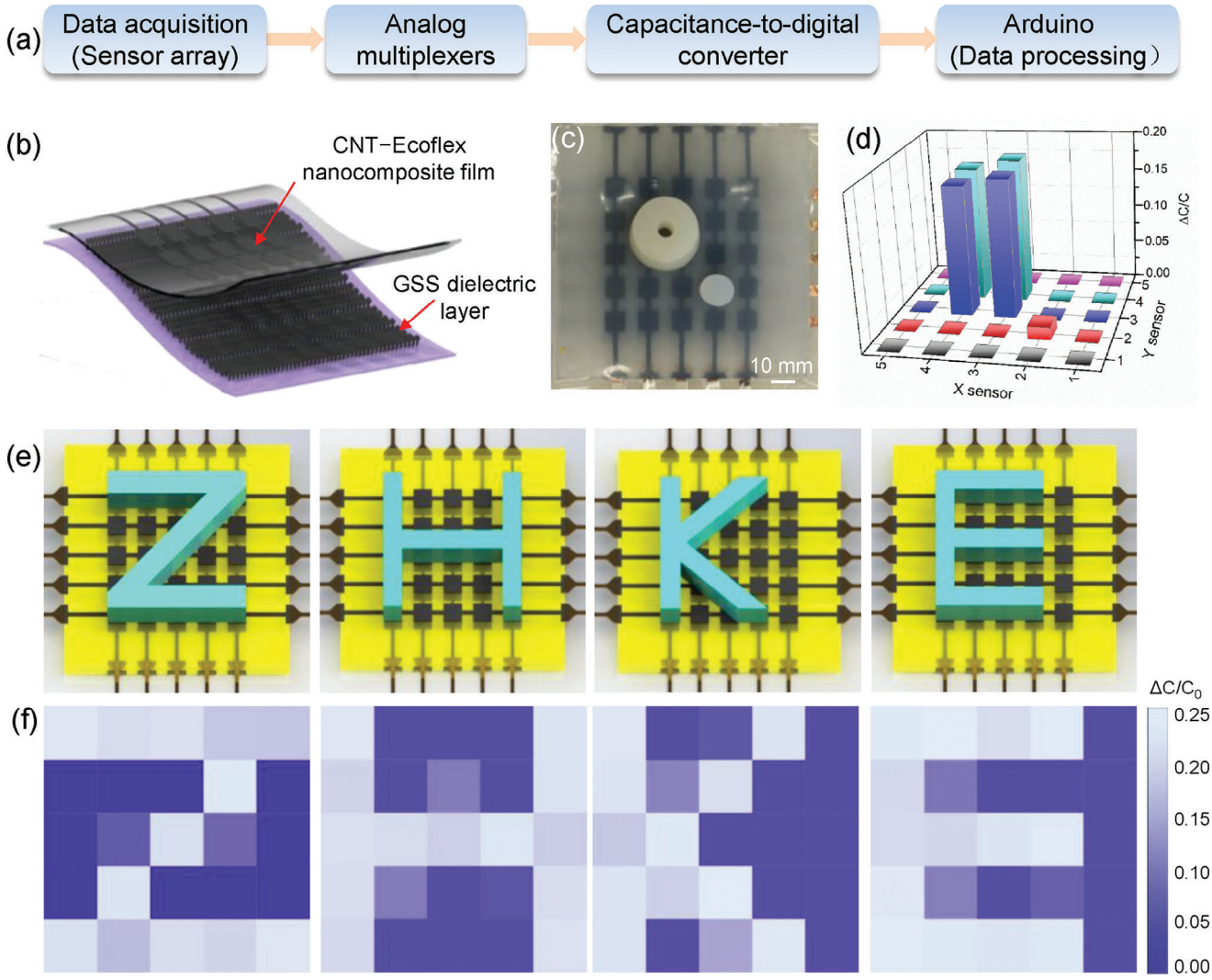

Figure 5. Demonstrations of the GSS-based capacitive pressure sensors in flexible perception array. a) Measurement system for pressure sensor array. b) The diagram of constructed flexible perception array. c) Sensor array pad placed with insulated objects featuring different weights (0.5 g and 6.0 g) and d) corresponding pressure distribution. e) The perception array placed with different letter blocks ("Z," "H," "K," and "E") and f) corresponding pressure distribution maps.

consistency of the fabricated GSS dielectric layer via 3D printing-based process, the capacitive pressure sensors exhibit a high sensor-to-sensor uniformity. Moreover, the experimental results indicate that the proposed GSS-based sensors present a high resolution over entire pressure range, an excellent dynamic response, a short response-relaxation time, a low hysteresis (<8%), a low detection limit (<3 Pa), and an outstanding long-term stability. Considering their superior performances, the GSS-based capacitive pressure sensors were applied in diverse application scenarios including external pressure stimuli detection, flexible perception array, and smart insole system. Therefore, we believe that this research offers a new strategy to endow flexible pressure sensors with extensive linearity range and excellent sensor-to-sensor uniformity. The novel design of the GSS dielectric layer can be promising for flexible pressure sensors in various applications, such as wearable electronics, environmental monitoring, and human–machine interfaces.

4. Experimental Section

Fabrication Process of GSS Dielectric Layer: Figure S2 (Supporting Information) schematically displays the fabrcation process of the GSS dielectric layer. First, master molds with sunken slant pillars were designed using Solidworks software, and then were sliced by Ultimaker Cura software. Next, the molds were fabricated by a fused deposition modeling-based 3D printer (Ulitmaker3, USA), and polyvinyl alcohol (PVA) was chosen as a printing material. Then, PDMS (Sylgard 184, Dow Corning Corporation, USA) with a 10:1 mass ratio of base to cross-linker and multiwalled carbon nanotubes (MWNTs; Carbon Nano-material Technology Co., Ltd., Korea) with an average diameter of ≈20 nm and average length of ≈5 µm were mixed using a planetary mixer, and the prepared prepolymer solution was poured into the printed molds. After removing the bubbles in a vacuum chamber for 2 h, the molds filled with PDMS-MWNTs prepolymer solutions were cured for 6 h at 60 °C. Afterwards, they were immersed in the DI water to dissolve the solidified PVA molds to obtain the GSS.

Preparation of CNT–Ecoflex Nanocomposite Film: First, the MWNTs were dispersed in isopropyl alcohol (IPA) solution through sonicating followed by stirring, and then the prepared CNT solution was spray-coated

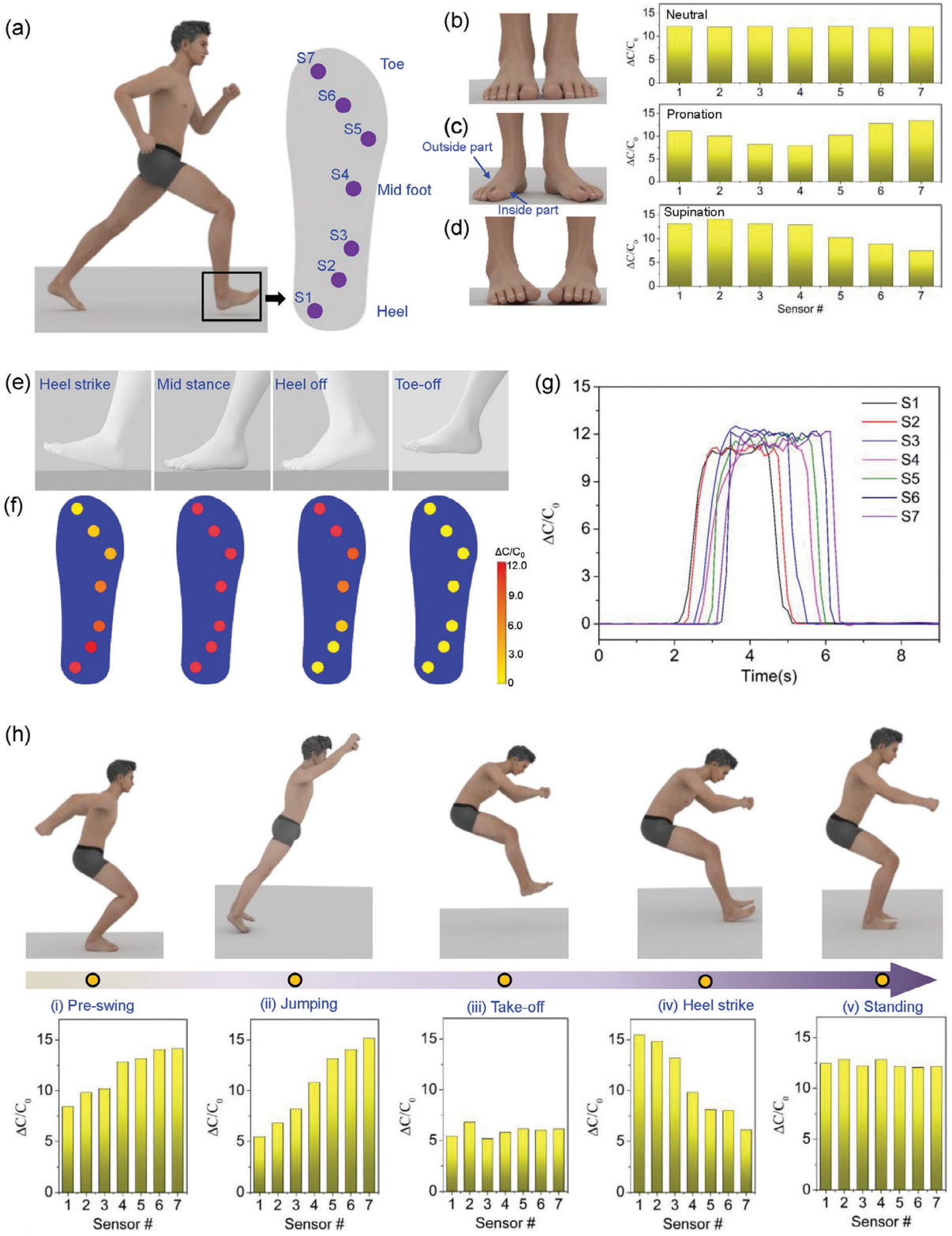

Figure 6. Demonstrations of the proposed pressure sensor in the smart insole. a) Seven pressure sensors on the sole, namely, S1-S7, to detect plantar pressure distribution. b–d) The normalized capacitive response for the seven pressure sensors under three different standing gaits (neutral, supination, and pronation). Here, the meaning of inside and outside part is annotated in (c). e,f) The schematic of a walking straight gait (heel strike, mid stance, heel off, and toe-off) and corresponding plantar pressure distribution. g) The capacitive response of the seven pressure sensors during a gait cycle. h) The evolution of relative capacitance changes of the seven pressure sensors during standing long jump (pre-swing, jumping, take-off, heel strike, and standing).

onto a substrate with a specific coating mask. After drying the CNT solution, the coating mask was removed. Subsequently, Ecoflex (Ecoflex Shore hardness 00–20, Smooth-On, Inc., USA) prepolymer solution (The mass ratio of part A and part B is 1:1) was poured onto the substrate with CNT patterns. Given that the Ecoflex prepolymer solution can penetrate the CNT network to generate a robust CNT–Ecoflex nanocomposite film, all CNT materials were located at the bottom of Ecoflex.[48] After curing it at 60 °C for 1 h, the Ecoflex film embedded with the CNT pattern was peeled off from the donor substrate. Next, the copper wires were connected to the end of CNT patterns using silver paste. Finally, the prepolymer solutions were poured again onto the CNT film surface and then curing it at 60 °C for 1 h, forming a CNT–Ecoflex nanocomposite film featuring a sandwich structure.

Finite Element Analysis Simulation: The deformation behavior of the GSS was simulated using Abaqus software. The simulation model was constructed by the actual size of fabriacted GSS dielectric layer. The material of the GSS dielectric layer was set as Mooney-Rivlin model with hyperelastic properties.[49]

Characterizations: A high-precision universal testing machine (AGS-X, SHIMADZU, Japan) was employed for compressing the pressure sensors, and the compression speed was fixed as 0.05 mm s^{-1}. The capacitance values of the pressure sensors were measured by an LCR meter (E4980A, Agilent, USA) under a frequency of 100 kHz. A capacitance-to-digital-converter board (EVAL-AD7746, Analog Devices Inc., USA) (Figure S16, Supporting Information) was utilized to measure the response-relaxation time of the GSS-based sensor.

Multisensor Measurement: The measurement system of the flexible perception array consists of a 5 × 5 capacitive sensor array, two analog multiplexers (CD4051BE, Texas Instrument, USA), a capacitance-to-digital converter (CDC, FDC1004, Texas Instruments, USA) (Figure S17, Supporting Information), and an Arduino Uno. The single eight-channel analog multiplexers were employed for cyclically scanning all sensors. The CDC instead of LCR meter was utilized to measure the capacitance values of the GSS-based sensors. For the smart insole system, the measurement system includes seven pressure sensors, two CDC boards, and an Arduino Uno. All experiments involving human subjects were conducted with the requisite approval from the Institutional Review Board (IRB) of the Korea Advanced Institute of Science and Technology (KAIST), under the reference number KH2023-001. Furthermore, informed written consent was obtained from all participants in these studies.

Supporting Information

Supporting Information is available from the Wiley Online Library or from the author.

Acknowledgements

This research was supported by the National Research Foundation of Korea (NRF) grant funded by the Korea government (MSIT) (No. 2021R1A2C3008742) and Alchemist Project grant funded by Korea Evaluation Institute of Industrial Technology (KEIT) and the Korea Government (MOTIE) (Project Number: 1415179744, 20019169). This work was also supported by National Natural Science Foundation of China (52175549).

Conflict of Interest

The authors declare no conflict of interest.

Data Availability Statement

The data that support the findings of this study are available from the corresponding author upon reasonable request.

Keywords

broad linearity range, capacitive pressure sensor, compressibility, gradient slant structures, sensor-to-sensor uniformity

Received: October 8, 2023
Revised: January 18, 2024
Published online:

[1] C. Hou, G. Tai, Y. Liu, R. Liu, X. Liang, Z. Wu, Z. Wu, *Nano Energy* **2022**, *97*, 107189.
[2] S. Zhuo, C. Song, Q. Rong, T. Zhao, M. Liu, *Nat. Commun.* **2022**, *13*, 1.
[3] Q. Zhang, D. Lei, N. Liu, Z. Liu, Z. Ren, J. Yin, P. Jia, W. Lu, Y. Gao, *Adv. Mater.* **2022**, *34*, 2205369.
[4] L. Wu, J. Ahn, J. Choi, J. Gu, X. Li, O. Gul, Z.-J. Zhao, L. Qian, B. Yu, I. Park, *Nano Energy* **2023**, *109*, 108299.
[5] Y. Jung, J. Choi, W. Lee, J. Ko, I. Park, H. Cho, *Adv. Funct. Mater.* **2022**, *32*, 2201147.
[6] S. Pyo, J. Lee, K. Bae, S. Sim, J. Kim, *Adv. Mater.* **2021**, *33*, 2005902.
[7] Z. Shi, L. Meng, X. Shi, H. Li, J. Zhang, Q. Sun, X. Liu, J. Chen, S. Liu, *Nano-Micro Lett.* **2022**, *14*, 1.
[8] Z. Nie, J. Kwak, M. Han, J. A. Rogers, *Adv. Mater.* **2022** 2205609.
[9] S. Zhao, W. Ran, D. Wang, R. Yin, Y. Yan, K. Jiang, Z. Lou, G. Shen, *ACS Appl. Mater. Interfaces* **2020**, *12*, 32023.
[10] J. Qin, L. Yin, Y. Hao, S. Zhong, D. Zhang, K. Bi, Y. Zhang, Y. Zhao, Z. Dang, *Adv. Mater.* **2021**, *33*, 2008267.
[11] H. Wang, Z. Li, Z. Liu, J. Fu, T. Shan, X. Yang, Q. Lei, Y. Yang, D. Li, *J. Mater. Chem. C* **2022**, *10*, 1594.
[12] S. Song, C. Zhang, W. Li, J. Wang, P. Rao, J. Wang, T. Li, Y. Zhang, *Nano Energy* **2022**, *100*, 107513.
[13] Y. Lee, J. Park, S. Cho, Y. Shin, H. Lee, J. Kim, J. Myoung, S. Cho, S. Kang, C. Baig, H. Ko, *ACS Nano* **2018**, *12*, 4045.
[14] C. Huang, G. Yang, P. Huang, J. Hu, Z. Tang, Y. Li, S. Fu, *ACS Appl. Mater. Interfaces* **2023**, *15*, 3476.
[15] J. Oh, J. Kim, Y. Kim, H. Choi, J. Yang, S. Lee, M. Pyatykh, J. Kim, J. Sim, S. Park, *Small* **2019**, *15*, 1901744.
[16] Y. Huang, X. Fan, S.-C. Chen, N. Zhao, *Adv. Funct. Mater.* **2019**, *29*, 1808509.
[17] X. He, Z. Liu, G. Shen, X. He, J. Liang, Y. Zhong, T. Liang, J. He, Y. Xin, C. Zhang, D. Ye, G. Cai, *npj Flexible Electron.* **2021**, *5*, 17.
[18] K. Cao, M. Wu, J. Bai, Z. Wen, J. Zhang, T. Wang, M. Peng, T. Liu, Z. Jia, Z. Liang, L. Jiang, *Adv. Funct. Mater.* **2022**, *32*, 2202360.
[19] L. Gao, M. Wang, W. Wang, H. Xu, Y. Wang, H. Zhao, K. Cao, D. Xu, L. Li, *Nano-Micro Lett.* **2021**, *13*, 140.
[20] R. Li, Q. Zhou, Y. Bi, S. Cao, X. Xia, A. Yang, S. Li, X. Xiao, *Sens. Actuators, A* **2021**, *321*, 112425.
[21] S. Mannsfeld, B. Tee, R. Stoltenberg, C. Chen, S. Barman, B. Muir, A. Sokolov, C. Reese, Z. Bao, *Nat. Mater.* **2010**, *9*, 859.
[22] D. Kwon, T. Lee, J. Shim, S. Ryu, M. Kim, S. Kim, T. Kim, I. Park, *ACS Appl. Mater. Interfaces* **2016**, *8*, 16922.
[23] Y. Guo, S. Gao, W. Yue, C. Zhang, Y. Li, *ACS Appl. Mater. Interfaces* **2019**, *11*, 48594.
[24] Y. Luo, J. Shao, S. Chen, X. Chen, H. Tian, X. Li, L. Wang, D. Wang, B. Lu, *ACS Appl. Mater. Interfaces* **2019**, *11*, 17796.
[25] Z. Qiu, Y. Wan, W. Zhou, J. Yang, J. Yang, J. Huang, J. Zhang, Q. Liu, S. Huang, N. Bai, Z. Wu, W. Hong, H. Wang, C. Guo, *Adv. Funct. Mater.* **2018**, *28*, 1802343.
[26] X. Zeng, Z. Wang, H. Zhang, W. Yang, L. Xiang, Z. Zhao, L. Peng, Y. Hu, *ACS Appl. Mater. Interfaces* **2019**, *11*, 21218.
[27] N. Bai, L. Wang, Y. Xue, Y. Wang, X. Hou, G. Li, Y. Zhang, M. Cai, L. Zhao, F. Guan, X. Wei, C. Guo, *ACS Nano* **2022**, *16*, 4338.

[28] B. Ji, Q. Zhou, M. Lei, S. Ding, Q. Song, Y. Gao, S. Li, Y. Xu, Y. Zhou, B. Zhou, *Small* **2021**, *17*, 2103312.
[29] N. Bai, L. Wang, Q. Wang, J. Deng, Y. Wang, P. Lu, J. Huang, G. Li, Y. Zhang, J. Yang, K. Xie, X. Zhao, C. Guo, *Nat. Commun.* **2020**, *11*, 1.
[30] T. Li, P. Pan, Z. Yang, J. Wei, X. Yang, J. Liu, J. Zhou, X. Zhang, G. Liu, *Adv. Mater. Technol.* **2022**, *7*, 2101135.
[31] J. M. R. Bullock, W. Federle, *Naturwissenschaften* **2011**, *98*, 381.
[32] J. Choi, D. Kwon, K. Kim, J. Park, D. Orbe, J. Gu, J. Ahn, I. Cho, Y. Jeong, Y. Oh, I. Park, *ACS Appl. Mater. Interfaces* **2019**, *12*, 1698.
[33] Y. Zheng, T. Lin, N. Zhao, C. Huang, W. Chen, G. Xue, Y. Wang, C. Teng, X. Wang, D. Zhou, *Nano Energy* **2021**, *85*, 106013.
[34] J. E. Han, D. Kim, K. S. Yun, *Sens. Actuators, A* **2012**, *188*, 89.
[35] S. Rachel, A. Ruthand, Z. Bao, *ACS Appl. Mater. Interfaces* **2020***12*, 58301.
[36] Z. Hu, Z. Chu, G. Chen, J. Cui, *IEEE Sens. J.* **2023**, *23*, 21040.
[37] S. Masihi, M. Panahi, D. Maddipatla, A. J. Hanson, A. K. Bose, S. Hajian, V. Palaniappan, B. B. Narakathu, B. J. Bazuin, M. Z. Atashbar, *ACS Sens.* **2021**, *6*, 938.
[38] S. R. A. Ruth, L. Beker, H. Tran, V. R. Feig, N. Matsuhisa, Z. Bao, *Adv. Funct. Mater.* **2020**, *30*, 1903100.
[39] A. Chhetry, S. Sharma, H. Yoon, S. Ko, J. Y. Park, *Adv. Funct. Mater.* **2020**, *30*, 1910020.
[40] S. Sharma, A. Chhetry, M. Sharifuzzaman, H. Yoon, J. Y. Park, *ACS Appl. Mater. Interfaces* **2020**, *12*, 22212.
[41] J. Huang, X. Tang, F. Wang, Z. Wang, Y. Niu, H. Wang, *Adv. Eng. Mater.* **2022**, *24*, 2101767.
[42] X. Fu, J. Zhang, J. Xiao, Y. Kang, L. Yu, C. Jiang, Y. Pan, H. Dong, S. Gao, Y. Wang, *Nanoscale* **2021**, *13*, 18780.
[43] C. Mahata, H. Algadi, J. Lee, S. Kim, T. Lee, *Measurement* **2020**, *151*, 107095.
[44] H. Kou, L. Zhang, Q. Tan, G. Liu, H. Dong, W. Zhang, J. Xiong, *Sci. Rep.* **2019**, *9*, 3916.
[45] J. Qiu, X. Guo, R. Chu, S. Wang, W. Zeng, L. Qu, Y. Zhao, F. Yan, G. Xing, *ACS Appl. Mater. Interfaces* **2019**, *11*, 40716.
[46] C. Ma, D. Xu, W. F. Liu, T. Y. Dong, S. T. Li, *IEEE Electron Device Lett.* **2021**, *42*, 1536.
[47] J. Xu, H. Li, Y. Yin, X. Li, J. Cao, H. Feng, W. Bao, H. Tan, F. Xiao, G. Zhu, *npj Flexible Electron.* **2022**, *6*, 62.
[48] M. Amjadi, Y. J. Yoon, I. Park, *Nanotechnology* **2015**, *26*, 375501.
[49] J. Woo, H. Lee, C. Yi, J. Lee, C. Won, S. Oh, J. Jekal, C. Kwon, S. Lee, J. Song, B. Choi, K.-I. Jang, T. Lee, *Adv. Funct. Mater.* **2020**, *30*, 1910026.

